INVESTIGATION OF THE TENSILE/COMPRESSIVE RESIDUAL STRESSES IN AISI 4340 STEEL UNDER LOW-CYCLE FATIGUE LOADING

Marian A. Patrick, Jeremy F. Laliberté, and Xin Wang[1]

[1] Carleton University, 1125 Colonel by Drive, Ottawa ON, K1V 6N2
marypatrick@cmail.carleton.ca

Abstract: Landing gear fuse pins are notched energy-absorbing mechanical components designed to reduce the possibility of aircraft structural damage in the event of a hard landing. The pins are sized to fracture when a predetermined load is exceeded during at a hard landing event. The area surrounding a fuse pin notch is in a state of complex stress, causing local yielding under applied loading. This work utilizes the strain-life method to study the low-cycle fatigue life of notched AISI 4340 steel components and to study the effects of complex residual stresses. This study involved quasi-static mechanical property testing, finite element analysis (FEA) simulation, and low-cycle fatigue testing of notched specimens. Control specimens were subjected to quasi-static low-cycle fatigue using the strain-life model. Variable specimens were subjected to either a quasi-static initial overload prior to fully reversed low-cycle fatigue loading, or a mean stress of identical magnitude as the residual stress induced from the applied overload. The magnitude of the residual stress at the notch root was determined using elastic-plastic FEA in ABAQUS-2021x. It was found that the tensile residual stress induced through compressive overload caused a 23% decrease in fatigue life, while the compressive residual stress induced by tensile overload caused a 5% increase in fatigue life. The residual stress was approximated as a mean stress to determine the suitability of this approximation as a design assumption. It was found that equating the tensile residual stress as a positive mean stress caused a reduction in estimated fatigue life to provide a conservative life estimate. However, equating the compressive residual stress to a negative mean stress for fatigue life predictions provided a highly non-conservative estimate. These results are significant in the design of components where plasticity must be considered in fatigue life assessments. Evaluation of the applicability of the residual stress to mean stress approximation is critical in ensuring conservative estimates are used in engineering applications.

Keywords: Stress concentration, FEA, residual stress, low-cycle fatigue, strain life

INTRODUCTION

Landing gear fuse pins, or shear pins, serve as a safety feature within aircraft landing gear systems. Fuse pins are designed as energy-absorbing components to allow for a controlled separation of the landing gear from the airframe in the event of a hard landing. Without the fuse pin, these events are more likely to cause a full collapse of the landing gear, resulting in extensive damage to the aircraft and potential injury to the passengers and crew. To properly absorb impact energy, fuse pins are designed as hollow

cylinders with an internal circumferential notch or groove to promote clean failure at a designated location (see Figure 1).
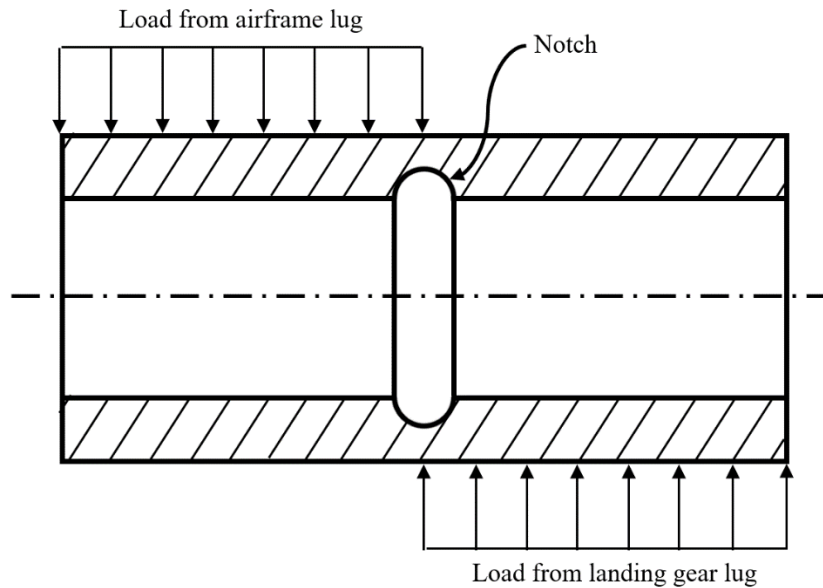

Figure 1: Simplified landing gear fuse pin cross-section in cantilever lug joint under single shear.

Fuse pins are designed to break only once a minimum threshold force is experienced when landing, however the inclusion of notches can cause components to fail prematurely. This premature failure is especially difficult to prevent when considering fatigue loading with unpredictable loading cases, such as overload. Overload is defined as an applied load exceeding the nominal yield point of a material (forming residual stress) with a maximum stress higher than the peak stress before or after the overload. To accurately design connective fuse pins, the low-cycle fatigue life with or without significant residual stress must be reliably estimated.

Residual stress is defined as the stress remaining in a material once an external load has been removed. Due to manufacturing processes, most components contain internal residual stresses which may compromise part longevity. The fatigue life of components with residual stresses induced by machining [1, 2], cold rolling processes [3], grinding [4], and shot peening [5–8] have been studied extensively. For steel under high-cycle fatigue conditions, compressive residual stresses have been found to increase component fatigue life, while tensile residual stresses decrease component fatigue life and should be avoided using careful manufacturing processes [9]. However, little research has been completed on the effects of residual stresses on low-cycle fatigue life. It is generally thought that the strains responsible for residual stresses tend to be inundated by the amplitude of the cyclic plastic strains under low-cycle fatigue loading [10]. One of the objectives of this paper is to investigate the effects of tensile and compressive residual stresses for notched samples of AISI 4340 steel.

To account for the effect of mechanically induced residual stresses in fatigue life predictions, a common design assumption is to equate a residual stress in a component with a stress riser to the local mean stress [11]. However, little research has been conducted on the effects of residual stresses and the validity of this residual stress approximation in the low-cycle fatigue regime [11].

This research investigates the effects of residual stress induced by overloads on the low-cycle fatigue life of AISI 4340 steel; a material commonly used in aircraft landing gear systems. Additionally, load-controlled experimental results with a local mean stress equivalent in magnitude to the local residual stress are compared to the Smith-Watson-Topper and the Morrow mean stress correction models. The approximation of equating the mean stress to the residual stress for fatigue life determination is assessed.

METHODOLOGY

The experimental methodology involved specimen design, monotonic tensile testing, finite element analysis simulations, and low-cycle fatigue testing.

Specimen Design

To meet the objectives of the study, round tensile specimens and notched fatigue specimens were manufactured. AISI 4340 annealed steel with the chemical composition given in Table 1 was procured as a 12.7 mm (0.5 in.) round bar and machined to size as per Figure 2. The fatigue coupon design was based on specimens from previous studies [11]. The material was tested in the 'as-received' state with no additional heat treatments or microstructural modifications.

Table 1: Chemical composition of AISI 4340 (wt%).

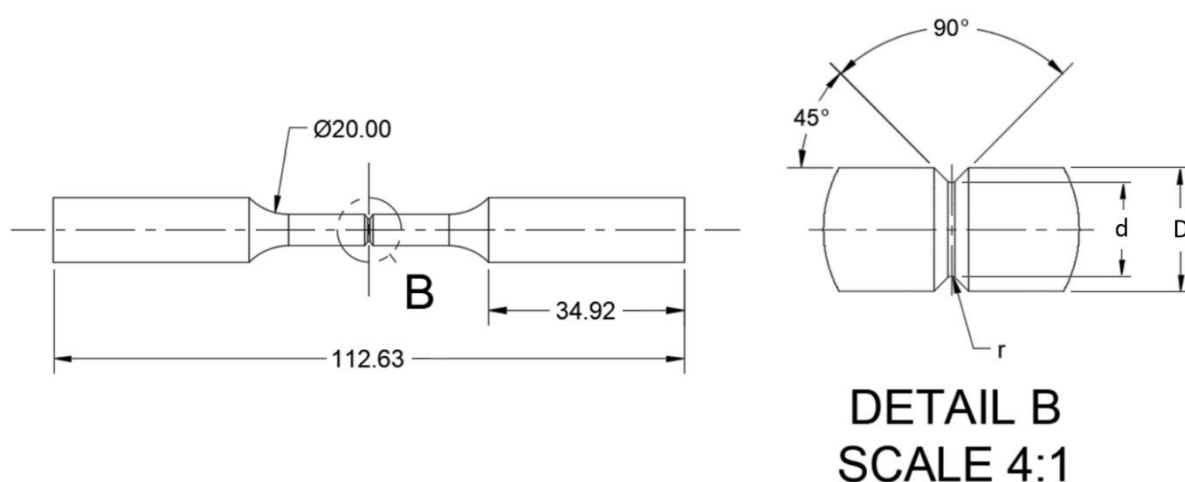| Al	C	Cr	Cu	Fe	Mn	Mo	Nb	Ni	P	S	Si	Sn	V
0.027	0.410	0.800	0.120	Bal.	0.720	0.210	0.002	1.760	0.011	0.023	0.27	0.007	0.002

Figure 2: Fatigue specimen dimensions.

Fatigue coupons were designed with a sharp v-notch in the center of the gage section to promote failure at the notch. The dimensions pertaining to the notch and the stress concentration factor are shown in Table 2. The stress concentration factor associated with the v-notch under axial loading was found to be 3 according to the process outlined in [12] which was used for the analytical portion of this work.

Table 2: Sample dimensions at the notch.

Dimension	Symbol	Value
Notch root diameter (mm)	d	4.13
Gage section diameter (mm)	D	5.51
Notch root radius (mm)	r	0.2032
Stress concentration factor	K_t	3.0

A finite element analysis (FEA) model was developed to relate the local strain amplitude at the notch root to the global force applied at the ends of the sample.

Finite Element Analysis Model

To build the relationship between local strain amplitude and global force amplitude, an axisymmetric model was created using ABAQUS 2021x [13] with a cross section of the sample defined in Figure 2. A material model was created by including the material properties summarized in Table 3 and the stress-strain data from tensile testing. The model was validated by comparing the stress concentration factor K_t obtained from the model to that given in Table 2. The K_t value from the model was found to be within 0.5% of the analytically determined result. Additionally, the material model was validated by

comparing the tensile data obtained from the model to the experimentally determined result. The stress-strain behaviour was found to correlate with the FEA stress-strain curve with a root mean square error (RMSE) value of 2×10^{-6}.

Boundary conditions (BC), loads, and constraints were applied to the finite element model as shown in Figure 3. Two symmetry boundary conditions were assigned to reflect axial symmetry about the longitudinal axis and symmetry about the axis containing the notch cross-sectional area. A rigid body constraint was placed along the grip section and a reference point with a tie constraint was attached to the grip end of the sample. A load and a boundary condition were both defined at the reference point such that the end could only move vertically (to the left in Figure 3.) in the direction of the applied load.
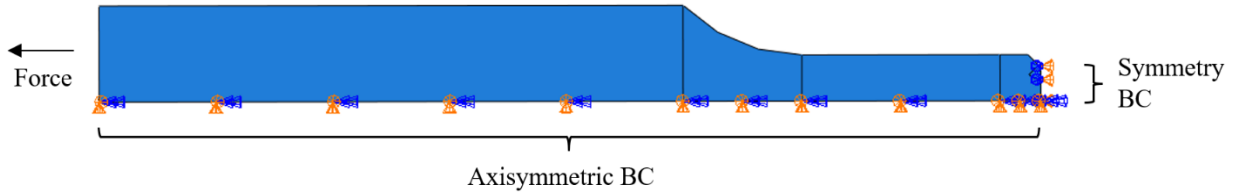

Figure 3: Finite element model with constraints, boundary conditions, and a defined load.

The FEM was partitioned into five distinct regions to allow for local mesh refinement. The mesh was created using a free meshing technique with quadrilateral elements aside from at the notch root, where the mesh was assigned using a swept meshing technique. The generated mesh is shown in Figure 4.
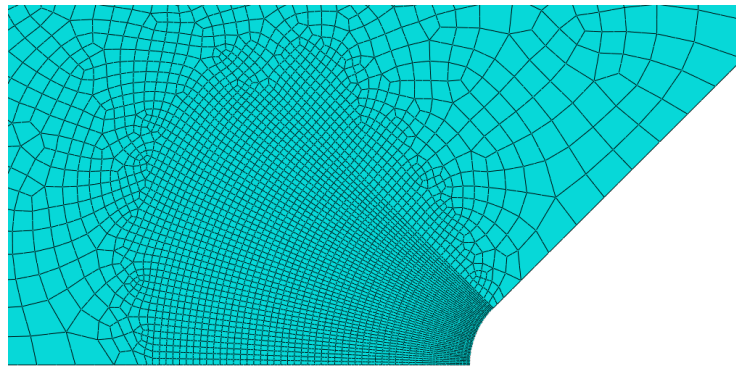

Figure 4: Notch root partition region of finite element model with swept mesh.

To validate the mesh, a convergence study was completed such that the maximum stress at the notch root was within 0.1% of the previous result. The convergence study rendered a total of 30686 elements in the model with a global seed size of 0.1 mm and a local seed size at the notch root of 1.7×10^{-2} mm. For the purposes of this investigation, the FEA results have been simplified to consider stress at the notch root as the uniaxial normal (S22) component.

Strain Life and Mean Stress Correction Models

Low cycle fatigue is fatigue in which plastic strains are dominant in the cyclic strain of a component, typically causing failure between 10^3 and 10^4 loading cycles. Fatigue life predictions in the low-cycle regime utilize the strain-life method to account for plasticity induced in each loading cycle. The strain amplitude required to cause failure in a given number of cycles is expressed using the strain life equation according to Eqn. 1,

$$\frac{\Delta \varepsilon}{2} = \underbrace{\frac{\sigma_f'}{E}\left(2N_f\right)^b}_{\text{elastic}} + \underbrace{\varepsilon_f'\left(2N_f\right)^c}_{\text{plastic}} \tag{1}$$

where $\frac{\Delta \varepsilon}{2}$ is the strain amplitude, σ_f' is the fatigue strength coefficient (MPa), E is the modulus of Elasticity (GPa), $2N_f$ is the number of reversals, b is the fatigue strength exponent, ε_f' is the fatigue

ductility coefficient, and c is the fatigue ductility exponent. The fatigue life parameters may be estimated using S-N curve data or, in the absence of S-N curve data, tensile data or hardness data as outlined in [14].

The strain-life method is suitable for fatigue life predictions under fully reversed proportional loading, however, it fails to account for non-zero mean stresses. Two widely used mean stress correction models are the Smith-Watson-Topper (SWT) model and the Morrow mean stress correction model. The SWT model adjusts Eqn. 1. by including the maximum tensile stress experienced during loading as shown in Eqn. 2. [15],

$$\sigma_{max} \frac{\Delta\varepsilon}{2} = \underbrace{\frac{{\sigma'_f}^2}{E}\left(2N_f\right)^{2b}}_{elastic} + \underbrace{\sigma'_f \varepsilon'_f \left(2N_f\right)^{b+c}}_{plastic} \tag{2}$$

Where $\sigma_{max} \frac{\Delta\varepsilon}{2}$ is the SWT damage parameter and σ_{max} is the maximum tensile stress during a loading cycle. This model has historically been applied to grey cast iron [16], hardened carbon steels [17, 18], some low-alloy steels [11], and micro-alloyed steels [19] with success. While the SWT model has proven to be useful when applied to other metals, it has demonstrated inaccuracies compared to other models when applied to AISI 4340 in the high-cycle fatigue regime [20].

The second mean stress correction is the Morrow equation, where the modification is made to the elastic strain term to account for an applied mean stress. The Morrow mean stress correction model is given by Eqn. 3 [21].

$$\frac{\Delta\varepsilon}{2} = \underbrace{\frac{\sigma'_f - \sigma_m}{E}\left(2N_f\right)^b}_{elastic} + \underbrace{\varepsilon'_f\left(2N_f\right)^c}_{plastic} \tag{3}$$

The Morrow mean stress correction has been successfully used in the high-cycle regime where elastic strain is dominant [14]. However, one significant shortfall of this model is the incorrect prediction of the ratio between the plastic strain range and the elastic strain range changing with mean stress. An additional shortcoming is the usage of two distinct curves with the Morrow model (one for a positive mean stress and one for a negative mean stress) with a significant difference in strain-life relationship between the two rather than one encompassing model.

Experimental Procedures
The experimental procedures for this study involved tensile testing, determination of strain life parameters, fully reversed fatigue testing, and fatigue testing with applied mean stresses and overloads.

Tensile testing was completed in accordance with ASTM E8 and ASTM A370 using standard round specimens [22, 23]. Six samples were tested at room temperature using a ±25 kN MTS 810 Material Testing System. An MTS 634.12E-24 class B-1 extensometer measuring the strain in the gage section was removed prior to specimen fracture to avoid damaging the equipment; thus, the ultimate tensile stress should be considered a lower-bound value. The average nominal true stress-strain behaviour is shown in Figure 5.
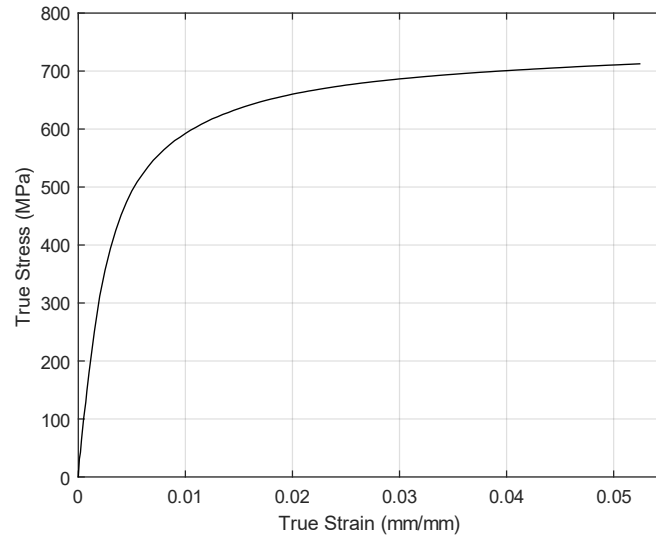
Figure 5: True stress-strain curve for AISI 4340 annealed steel.

The average tensile data was found using the stress-strain behaviour from Figure 5. The yield stress was found using the 0.2% offset method. The average tensile data with the standard uncertainty for AISI 4340 is included in Table 3.

Table 3: Tensile data for AISI 4340 annealed steel.

Tensile Parameter	Value
Ultimate tensile strength (MPa)	715 ± 8
0.2% offset yield strength (MPa)	470 ± 6
Modulus of elasticity (GPa)	190 ± 8
Percent reduction in area (%)	43 ± 1

The tensile test parameters from Table 3 were used to determine the strain life parameters given in Table 4 according to the methodology outlined in [14].

Table 4: Strain-life fatigue parameters for AISI 4340 annealed steel.

Fatigue Parameter	Symbol	Value
Fatigue strength coefficient (MPa)	$\sigma_f{}'$	985
Fatigue strength exponent	b	–0.079
Fatigue ductility coefficient	$\varepsilon_f{}'$	0.563
Fatigue ductility exponent	c	–0.513

The strain life parameters were used in Eqn. 1 to determine the strain amplitude required for failure in a given number of cycles under fully reversed loading. A relationship between the global force applied at the sample ends and the local strain at the notch root was developed using the finite element analysis model described previously.

Fatigue Testing
Fatigue testing was completed in accordance with ASTM E466 [9]. A total of six distinct loading conditions were tested using a ±25 kN MTS 810 Material Testing System with serrated wedge grips and a clamping pressure of 15 MPa. The setup of a fatigue coupon in the MTS is shown in Figure 6.

Figure 6: Experimental setup of notched AISI 4340 fatigue coupons.

The loading conditions for each sample number are outlined in Table 5. The load conditions described are the loads applied at the sample ends by the MTS software. It should be noted that R in Table 5 is defined as the stress ratio, or the ratio of the minimum stress to maximum stress for constant amplitude loading.

Table 5: Loading Conditions for Fatigue Testing

Sample #	Initial Overload (kN)	Mean Load (kN)	Maximum Load (kN)	R
1 – 3	0	0	7.00	−1.00
4 – 6	0	4.00	11.00	−0.27
7 – 9	0	−4.00	3.00	−3.67
10 – 12	11.00	0	7.00	−1.00
13 – 15	−11.00	0	7.00	−1.00

Tests were conducted at room temperature using load-control with a sinusoidal forcing function. To build on previous studies [11, 16], the feasibility of using strain life theories for load-controlled testing is investigated in this paper. One of the challenges of using load-controlled testing and applying the strain life theories is the lack of consideration for changes in strain due to loading. Under strain-controlled tests, the strain is at a constant amplitude which allows for the strain-life parameters to be constant. The strain life theories used in this paper are derived from strain-controlled loading conditions and do not consider the change in strain amplitude with time associated with load-control. Thus, this paper aims to investigate the applicability of the strain life equations using load-control rather than strain-control loading.

Testing was completed at a loading rate of 2 cycles per minute, or an average approximate strain rate at the notch root of 2×10^{-3} s^{-1}, to study the rate-independent plastic deformation. Fully reversed testing was completed to provide a baseline for the comparison of mean stress and residual stress effects. A single initial overload was applied to the residual stress specimens over a period of 30 s and removed at the same rate for quasi-static load application. The mean stress was implemented using the MTS software. All specimen testing was completed to failure, where failure is defined as the complete separation of the specimen.

The residual stress to mean stress equivalence was established by applying and releasing a −11 kN load in the FEA model to produce a maximum residual stress of 900 MPa at the notch root. The notch root mean stress was set to be equal in magnitude to the residual stress, producing a nominal mean stress of 300 MPa, or a mean load of 4 kN. It should be noted that, while the maximum residual stress (S22) is larger than the yield strength, the area directly surrounding the notch root is in a state of complex triaxial stress. The residual stress decreases and stabilizes as the distance from the notch root is increased, as shown by Figure 7.
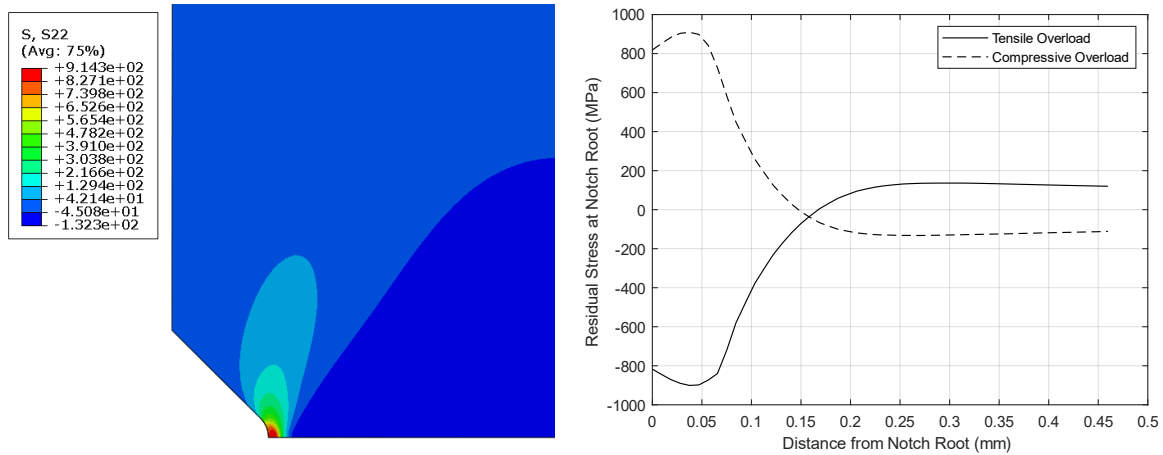

Figure 7: Tensile and compressive residual stress relative to distance from the notch root

RESULTS AND DISCUSSION

Based on preliminary calculations, to have the fatigue specimens fail at 1000 cycles under fully reversed loading, the required maximum strain at the notch root was found to be 0.015 mm/mm, corresponding to a load amplitude of 7 kN. A summary of experimental test results for the various load cases is given in Table 6. Three samples were tested for each load case and averaged to provide a final life cycle value.

Table 6: Low cycle fatigue test results for AISI 4340 annealed under various loading conditions.

Sample #	Residual Stress S22 (MPa)	Nominal Mean Stress (Notch Root) (Mpa)	Cycles to Failure	Average Cycles to Failure
1			1010	
2	0	0	907	966 ± 53
3			981	
4			452	
5	0	300 (900)	372	372 ± 81
6			291	
7			3356	
8	0	−300 (−900)	3698	3745 ± 415
9			4181	
10			1199	
11	−900	0	1038	1017 ± 193
12			815	
13			656	
14	900	0	742	767 ± 125
15			902	

The results tabulated above can alternatively be expressed visually as a function of mean or residual stress at the notch and cycles to failure, as shown in Figure 8.
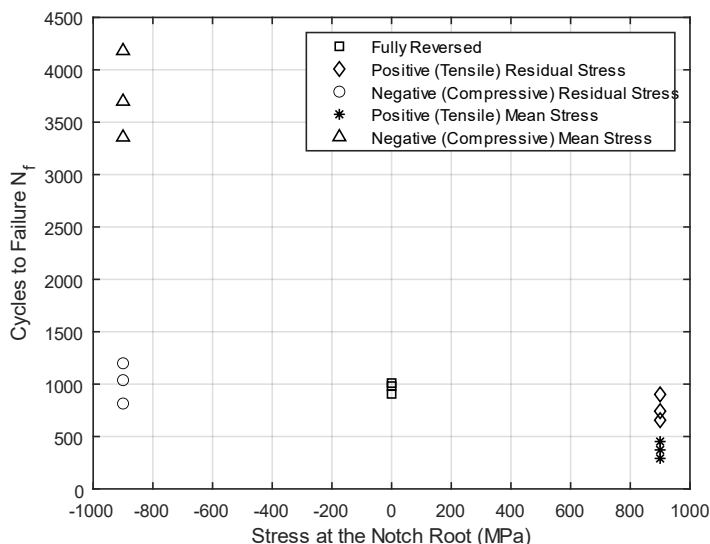
Figure 8: Mean/residual stress at the notch root vs number of cycles to failure.

Fully Reversed Loading

For fully reversed low-cycle fatigue, the average number of cycles to failure was 966 ± 53, which is a 3.5% difference compared to the predicted 1000 cycles. While the data set is small, this correlates well with findings in the literature for various materials [11, 16, 24] stating that the usage of strain-life equations with the first cycle of load-controlled testing is a suitable estimate for fatigue life prediction.

Mean Stress Effects

The average fatigue life for specimens under low-cycle fatigue loading with a positive (tensile) mean stress is 372 ± 81 cycles, or less than half of the zero mean stress baseline. The average life for the negative (compressive) mean stress samples is 3745 ± 415, which shows a nearly four-fold increase in life relative to the baseline samples. These results demonstrate that mean stresses have a significant effect on the fatigue life in the low-cycle fatigue regime for AISI 4340, which is consistent with previous literature [11]. The experimental fatigue life for tensile and compressive mean stress specimens was further compared to a) the SWT model and b) the Morrow mean stress correction shown in Figure 9. The average experimental fatigue data for each mean stress case is plotted and compared to the mean stress correction models. It should be noted that the error bars associated with the experimental data points correspond to the standard uncertainty of the respective result.
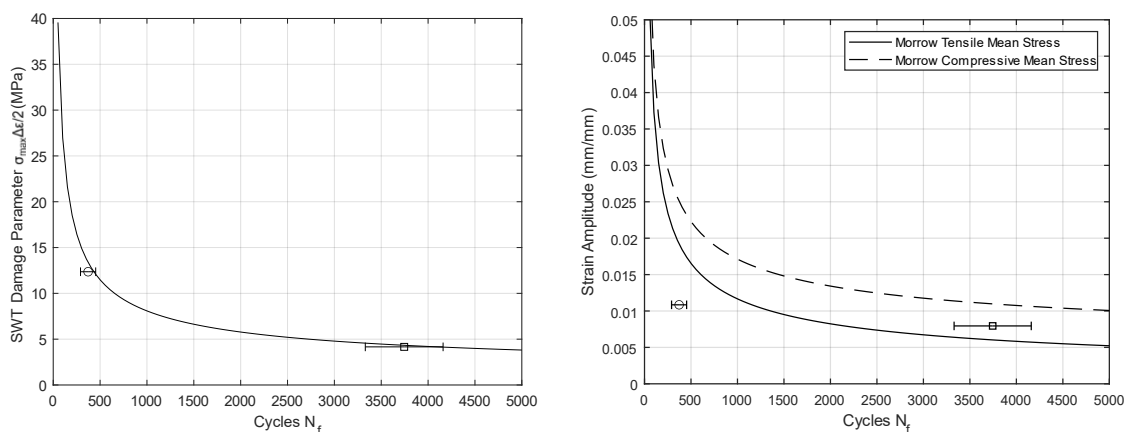

Figure 9: Experimental low cycle fatigue data for annealed AISI 4340 with tensile/compressive mean stress relative to the a) Smith-Watson-Topper model and b) Morrow model.

Comparing experimental results with mean stress correction models, the SWT model produces an error of percent difference of 14% for the estimated fatigue life of the tensile mean stress specimens and a percent difference of 9% for the life estimate of the compressive mean stress specimens. As noted from Figure 9, the SWT model provides a slightly nonconservative life estimate for both the tensile and compressive mean stress cases. The Morrow model presents a 100% difference for the tensile mean stress data and a 105% difference for the compressive mean stress data, providing highly nonconservative estimates for both mean stress cases. It should be noted that the correlations between experimental and modelled mean stresses are highly dependent on the fatigue ductility exponent c which is obtained from the literature [14], as the change from –0.513 to –0.6 produces a maximum percent difference in fatigue life of 5% using the Morrow mean stress correction model and a maximum percent difference of 66% using the SWT model, with both models providing conservative fatigue life estimates.

Residual Stress/Overload Effects

The samples with compressive residual stress (due to an initial tensile overload) failed at an average of 1017 ± 193 cycles. This is a slight (5%) improvement in fatigue life compared to fully reversed samples, however this result indicates that beneficial compressive residual stresses were relaxed throughout loading. The tensile residual stress samples failed at an average of 767 ± 125 cycles, providing a 23% decrease in fatigue life. While this is a small sample size (< 5), these results demonstrate that AISI 4340 may be particularly susceptible to tensile residual stresses decreasing the low-cycle fatigue life, while the benefit of compressive residual stresses under low-cycle fatigue life may be negligible. Further investigations should be conducted on varying the magnitude of the initial overload to determine if this negligible benefit is applicable for all overload ratios for AISI 4340 steel under low-cycle fatigue loading.

The approximation of equating residual stress to mean stress locally at the notch root demonstrates differences in experimental fatigue life depicted visually in Figure 8. Equating the tensile residual stress to a tensile mean stress is a conservative estimate, producing a percent difference in fatigue life of approximately 70%. However, equating the compressive residual stress to a compressive mean stress is highly nonconservative with a percent difference in fatigue life of approximately 120%.

Fractography

The fracture surfaces were captured using scanning electron microscopy (SEM). The fully reversed fracture surface for a baseline sample is given by Figure 10. Section a) shows the ductile cup-and-cone fracture surface at rupture with an outstretched surface and b) demonstrates the brittle crack propagation region given by a relatively flat surface.
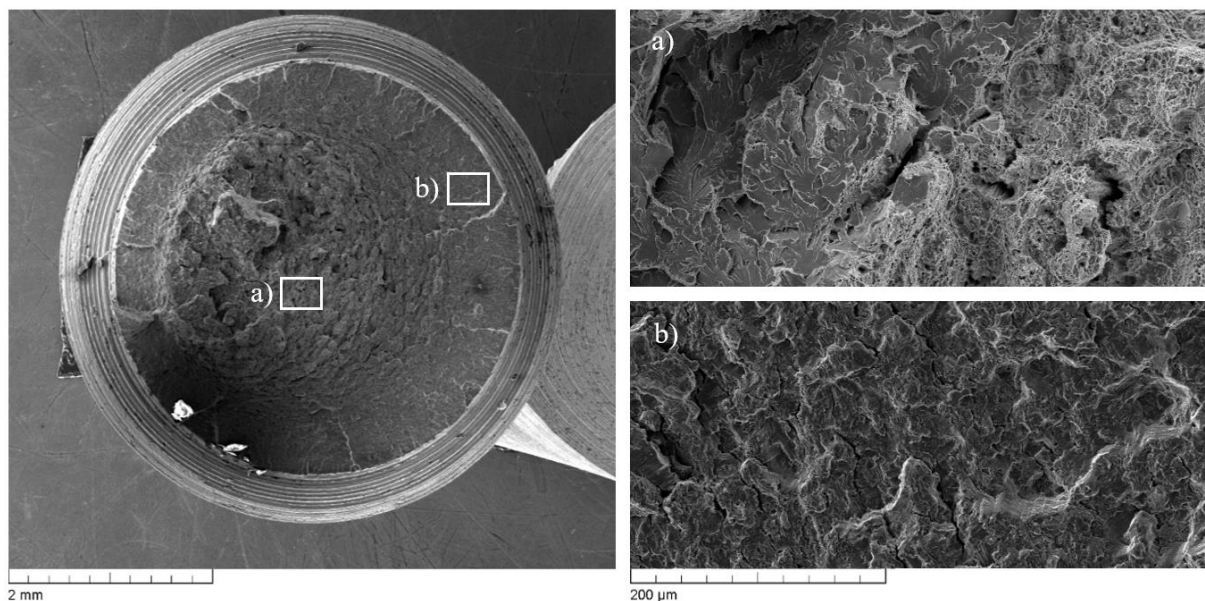

Figure 10: SEM images for a fully reversed sample fracture surface.

Comparatively, the SEM images for the specimens with an applied initial overload or an applied mean stress are given by Figure 11.
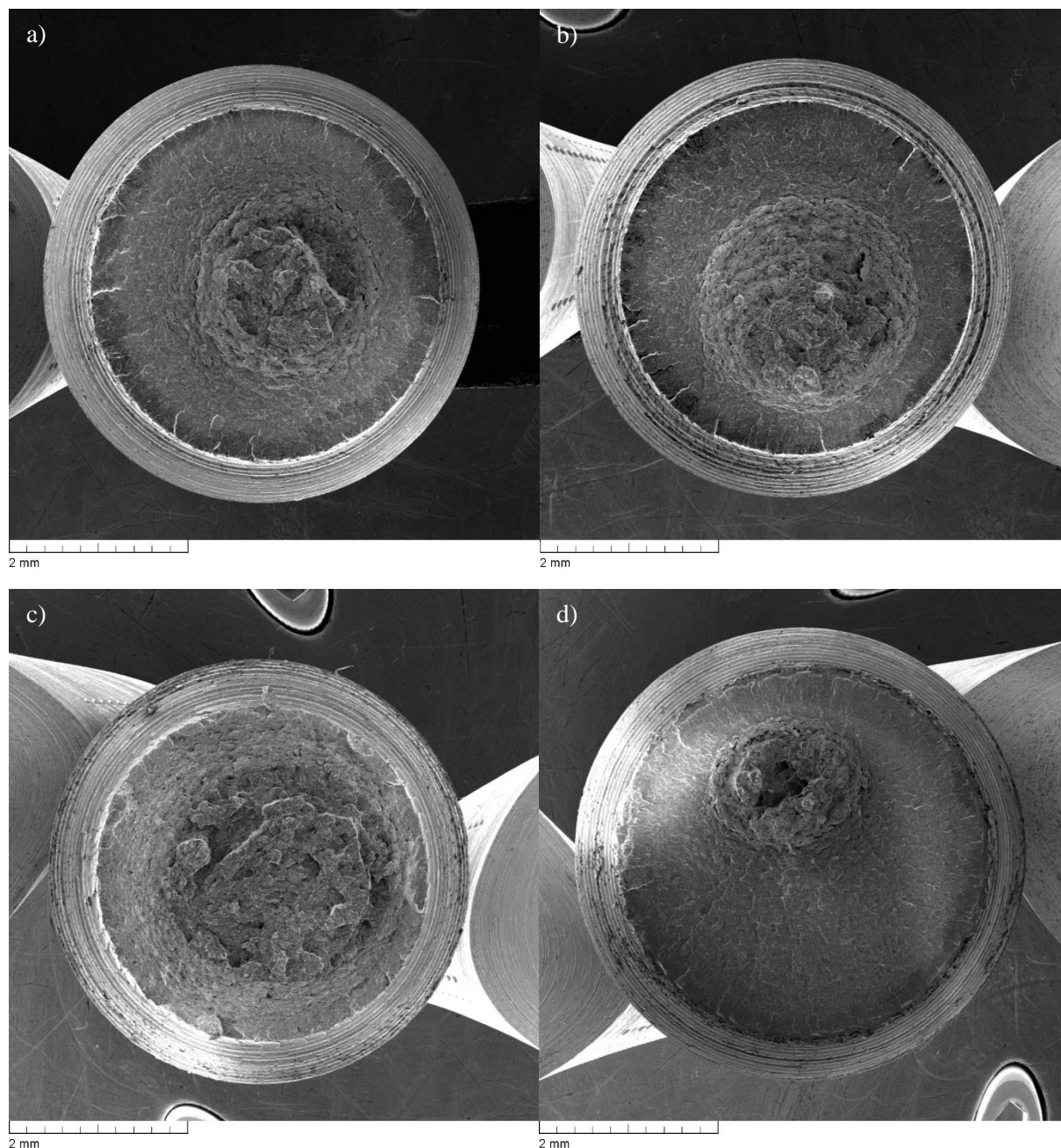

Figure 11: SEM images for specimens with a) a tensile overload, b) a compressive overload, c) a tensile mean stress, and d) a compressive mean stress

Given the fractographic results demonstrating the magnitude of time spent in the crack propagation period, it may be of interest to determine the effects of periodic overloads in the low-cycle regime. The SEM images demonstrate no significant change in fracture surface characteristics due to the tensile or compressive overload compared to baseline samples. Since the crack propagation regions and fracture areas are identical, the effects of the initial overloads on fatigue life affected the crack initiation phase.

The mean stress coupons demonstrate a significant change in fatigue life which is noted by the size of the rupture area and the length of the crack propagation region. Figure 11 c) shows a tensile mean stress coupon with a large rupture region and small crack propagation region. It is expected that the rupture area would be larger due to the increased maximum stress applied to the coupon compared to fully

reversed loading. Additionally, the entire fracture surface shows significant plasticity under loading through outstretched grains. Alternatively, the compressive mean stress coupon has a much smaller rupture area (due to a smaller maximum stress experienced in the coupon) with a much larger crack propagation region. This increased crack propagation region is proportional to the increase in low-cycle fatigue life and inversely proportional to the rupture area. The effect of mean stress changing the size of the crack propagation region is distinct from the initial overloads affecting the crack initiation region. This difference further denotes the usage of the design assumption equating residual stress to a mean stress for fatigue life approximations.

CONCLUSION

This paper investigated the residual stress effects of AISI 4340 annealed steel under low-cycle fatigue loading. The following conclusions can be made from the results:

1. The approximation of equating the local residual stress as a mean stress for low-cycle fatigue life analysis of notched AISI 4340 steel is generally a nonconservative estimate and should be avoided.
2. Fatigue life results from load-controlled testing demonstrated good agreement with strain life methodologies. While the sample size is small, this correlates well with the literature supporting load control.
3. The Smith-Watson-Topper model and the Morrow mean stress correction model both provided nonconservative estimates for tensile mean stress and compressive mean stress coupons. However, the Smith-Watson-Topper correction provided more accurate fatigue life predictions in the low-cycle fatigue regime compared to the Morrow model, with a maximum percent difference of 14% between the predicted fatigue life and experimental result. Predictive results are highly dependent on fatigue ductility exponent c in the low-cycle fatigue regime.
4. Fractographic analysis demonstrated that the effect of initial overloads had an impact in only the crack initiation phase. The low-cycle fatigue life of mean stress coupons is found to be proportional to the size of the crack propagation region or inversely proportional to the rupture area.

The results from this research are significant in engineering design applications involving rate-independent plasticity or under low-cycle fatigue loading conditions. These findings should be considered in the design of components with stress risers, such as landing gear fuse pins, where unexpected loading conditions in combination with fatigue loading may compromise part performance.

ACKNOWLEDGEMENTS

REFERENCES

[1] Wan, M., Ye, X.-Y. and Zhang, W. H. (2019), *J. Mater. Sci.,* vol. 54, p. 1-35.
[2] Sasahara, H. (2005), *Int. J. Mach. Tools Manuf.,* vol. 45, n. 2, p. 131-136.
[3] Horger, O. J. (1935), *J. Appl. Mech.,* vol. 2, n. 4, p. 128-136.
[4] Matsumoto, Y., Magda, D., Hoeppner, D. and Kim, T. Y. (1991), *J. Eng. Ind.,* vol. 113, n. 2.
[5] Townsend, P. and Zaretsky, E. V. (1982), NASA TP-2047, National Aeronautics and Space Administration, Hampton.

[6] Landgraf, R. W., Chernenkoff, R. A. (1988). In: *Analytical and Experimental Methods for Residual Stress Effects in Fatigue*, ASTM STP 1004, pp. 1-12, R. L. Champoux, J. H. Underwood, and J. A. Kapp (Eds.), American Society for Testing and Materials, Philadelphia.

[7] Mattson, R. L. (1954), *SAE trans.*, vol. 62, p. 416-425.

[8] Dowling, N. E. (2012). In: *Mechanical Behaviour of Materials, Engineering Methods for Deformation, Fracture and Fatigue (4th ed.)*, pp. 536, Pearson Education Ltd., Harlow.

[9] ASTM International (2015). In: *ASTM E466-15 Standard Practice for Conducting Force Controlled Constant Amplitude Axial Fatigue Tests of Metallic Materials,* ASTM, West Conshohocken.

[10] Withers, J. P. (2007), *Rep. Prog. Phys.*, vol. 70, p. 2211-2264.

[11] Bassindale, C., Wang, X. and Miller, R. E. (2020), *Int. J. Fatigue*, n. 130, 105273.

[12] Pilkey, W. D., Pilkey, D. F. and Bi Z. (2020). In: *Peterson's Stress Concentration Factors* (4th ed.)*,* pp. 132, John Wiley & Sons Inc.*,* Hoboken.

[13] Dassault Systèmes (2011). In: *ABAQUS/CAE User's Manual*, Dassault Systèmes Simulia Corp., Providence.

[14] Lee, Y.-L., Pan, J., Hathaway, R. and Barkey, M. (2005). In: *Fatigue Testing and Analysis (Theory and Practice),* pp. 219-220, Elsevier, Burlington.

[15] Smith, K. N., Watson, P. and Topper, T. H. (1970), *J. Mater.*, vol. 5, n. 4, p. 767-778.

[16] Fash, J. and Socie, D. F. (1982), *Int. J. Fatigue.*, vol. 4, n. 3, p. 137-142.

[17] Koh, S. K. and Stephens, R. I. (1991), *Fatigue Fract. Eng. Mater. Struct.*, vol. 14, n. 4, p. 413-428.

[18] Wehner, T. and Fatemi, A. (1991), *Int. J. Fatigue*, vol. 13, n. 3, p. 241-248.

[19] Forsetti, P. and Blasarin, A. (1988), *Int. J. Fatigue*, vol. 10, n. 3, p. 153-161.

[20] Badr, E. A. and Ishak, J. (2021), *Int. J. Press. Vessel. Pip.*, vol. 194B.

[21] Morrow, J. D. (1965). In: *Internal Friction, Damping, and Cyclic Plasticity*, ASTM STP 378, pp. 45-68, American Society for Testing and Materials, Philadelphia.

[22] ASTM International (2022). In: *ASTM E8/E8M-22 Standard Test Methods for Tension Testing of Metallic Materials,* ASTM, West Conshohocken.

[23] ASTM International (2022). In: *A370-22 Standard Test Methods and Definitions for Mechanical Testing of Steel Products,* ASTM, West Conshohocken.

[24] Colin, J., Fatemi, A. and Taheri, S. (2010), *J. Eng. Mater. Technol.,* vol. 132, n. 2, 021008.